Numerical Investigation of a 7-Element GOX/GCH4 Rocket Combustion Chamber

By D. Eiringhaus, D. Rahn†, H. Riedmann AND O. Knab

ArianeGroup GmbH
Robert-Koch-Straße 1, 82024 Taufkirchen, Germany

In recent years the use of the propellant combination methane and oxygen in liquid propellant rocket engines has emerged as research topic of interest in both industry and academia due to its suitability to reuseability and potential for cost reduction. In the frame of the 2017 Summer Program of the Collaborative Research Center SFB-TRR 40, the water cooled calorimetric 7-element GOX/GCH4 rocket combustion chamber of the Institute of Turbomachinery and Flight Propulsion was chosen as a common test case for combustion and heat transfer analysis tools. ArianeGroup participated with its new Rocflam3 solver, an industrial spray combustion and heat transfer analysis tool in three spatial dimensions, employing the newly implemented adiabatic flamelet model for combustion modeling. The numerical setup including the utilized models and computational grid are presented. Results are given for stand-alone simulations of the combustion side in 2D and 3D with an investigation into turbulence modeling and chemistry tabulation as a function of pressure. A one-way coupled analysis of the coolant flow in the cooling channels and heat conduction in the combustion chamber hardware using Ansys CFX is present as a starting point for future the future fully coupled hot gas - cooling side simulations.

1. Introduction

In most space faring nations the use of the propellant combination of liquid oxygen (LOX) and liquid methane (CH4) in future rocket engines is a topic of high interest. Cost has become a major factor in design optimization with the emergence of new players on the space launcher market. The application of hydrocarbons and especially methane as rocket fuel has been identified in the frame of the European Future Launcher Preparatory Programme (FLPP) [1, 2] as a means to obtain cheaper space launch systems. Research on LOX/CH4 was performed at ArianeGroup in concept studies of a full scale thrust chamber demonstrator in the 400 kN thrust range, starting in 2007. A hot fire test campaign was performed on the P3.2 test bench of the Deutsches Zentrum für Luft- und Raumfahrt (DLR) in Lampoldshausen, Germany and concluded successfully in 2016. An overview on the experiences gained during the test campaign is given by Blasi and Häberle [3].
Studies at ArianeGroup on the topic of next generation liquid rocket engine focus on heavy cost reduction and reusability and culminated in the definition of the Prometheus engine [4].

† also at Institute of Turbomachinery and Flight Propulsion, Technische Universität München

In the context of the Collaborative Research Center TRR40 "Fundamental Technologies for the Development of Future Space-Transport-System Components under High Thermal and Mechanical Loads", ArianeGroup aims to increase the performance of its numerical heat transfer and combustion analysis tools used in the design process. The 7-element sub-scale combustion chamber operated by the SFB's project K1 offers valuable experimental data for the validation of such tools. In the frame of the summer program 2017 ArianeGroup participated with its 3D RANS tool Rocflam3. A first status of the setup and application of different industrial tools including Rocflam3 is given by Eiringhaus et al. [5]. Here a global chemistry approach utilizing Magnussen's Eddy Dissipation Concept [6] for turbulence-chemistry interaction and a pPDF-equilibrium chemistry were used for combustion modeling. The latter was also used by Riedmann et al. [7] for the numerical simulation of sub-scale combustion chambers, showing good predictions of the wall heat flux while underestimating the combustion efficiency. A comprehensive comparison given by Roth et al. [8] of the results different research groups obtained over the course of the Summer Program 2015 on a GOX/GCH4 single-element chamber confirms the deficiencies of the available Rocflam3 modeling strategies at ArianeGroup regarding the prediction of all relevant aspects. Therefore, a new adiabatic flamelet model has since been implemented in Rocflam3 and was first applied to the 7-element chamber of the 2017 Summer Program. Setup and results for both stand-alone hot gas and coolant 3D CFD simulation are presented in the following.

2. Experimental Setup

In the following the main dimensions of the multi-element combustion chamber are presented. A detailed description of the hardware is given by Silvestri et al. [9]. The combustion chamber has a circular cross section with an inner diameter $d_{\text{cyl}} = 30$ mm and a contraction ratio $\varepsilon_c = 2{,}5$, resulting in a throat diameter $d_t = 19$ mm. The total length l of the combustion chamber from faceplate to exit plane is 383 mm. It is designed for combustion chamber pressures of up to 100 bar and a maximum combustion temperature of 3600 K. The hardware is manufactured from oxygen free high conductivity copper (OFHC-Cu) and comprises five water cooled segments of which four make up the cylindrical part of the combustion chamber and one contains the convergent divergent nozzle. A schematic view of the chamber layout is given in Figure 1. The first cylindrical segment has milled cooling channels with a rectangular cross section, comparable to the current cooling channel design in flight proven thrust chambers like

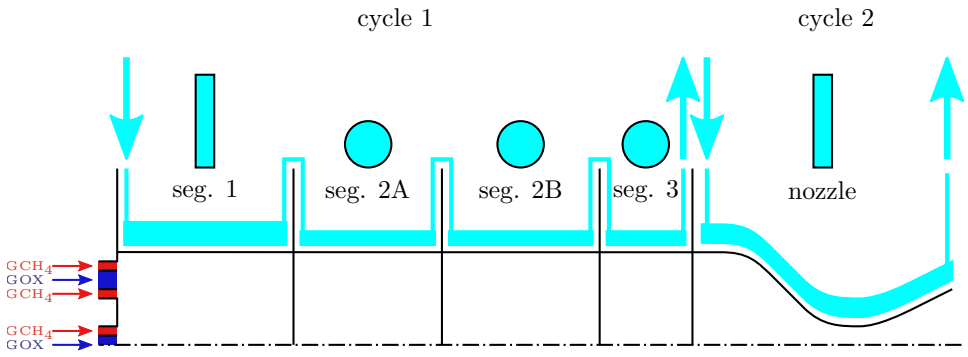

FIGURE 1. Schematic View of the 7-Element Combustion Chamber

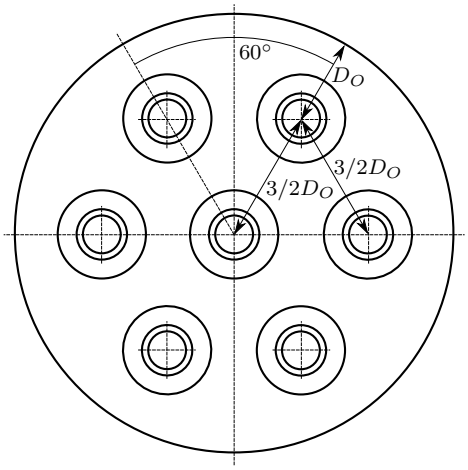

FIGURE 2. Schematic View of the 7-Element Injector

Dimension	Symbol	Unit	Value
combustion chamber diameter	d_{cyl}	mm	30,0
throat diameter	d_t	mm	19,0
total length	l	mm	383
characteristic length	$l*$	mm	906
divergence angle	α_{div}	°	15
GOX diameter	D_i	mm	4,0
GOX post wall thickness	t	mm	0,5
GOX post recess	r	mm	0,0
GOX post taper angle	α	°	0,0
GCH4 diameter	D_o	mm	6,0

TABLE 1. Main Chamber and Injector Dimensions

Vulcain 2 or HM7B. Segments 2A, 2B and 3 feature drilled cooling channels, which are both cheaper and easier in the manufacturing process. The cross section of the cooling channels in the nozzle segment is rectangular, like in segment 1. The coolant water is routed in two cycles. The first cycle enters the distribution manifold on the upstream end of segment 1 and is routed through segments 1, 2A, 2B and 3 where it leaves segment 3 on the downstream end. The second cycle is solely used for the cooling of the nozzle segment. As injection element, a coaxial-shear element with a central GOX post and an annular GCH4 sleeve is used. For the current experiments the GOX post is mounted flush with the faceplate and possesses no tapering. The injection pattern is shown in Figure 2 and exhibits a central element on the chamber axis and six equally spaced elements on a concentric circle with a radius of $3/2D_o$. This ensures that the injector-injector distance is constant for all elements. The main dimensions of the combustion chamber and the injection element are given in Table 1.

3. Numerical Setup

3.1. *Hot Gas Side*

For the simulation of the hot gas side ArianeGroup's in-house 3D spray combustion and heat transfer analysis tool Rocflam3 is used. Rocflam3 offers several combustion and turbulence models. For all presented simulations Menter's k-ω-SST model [10] is used for turbulence modeling and combustion is modeled using a adiabatic standard pPDF-flamelet model with its concept mainly advanded by Peters [11]. Within the current development process at ArianeGroup, this newly implemented combustion model has been adapted to allow for a pressure dependency of the chemistry tabulation. The symmetry of the combustion chamber is exploited and only a 60° segment is simulated. The used structured multi-block grid is depicted in Fig. 3 with the x-axis along the chamber axis and the definition of $x = 0$ in the throat section at the smallest diameter. During the grid generation special attention is given to the wall resolution and a dimensionless wall distance of $y^+ < 1$ is ensured. A detailed mesh study was performed by Eiringhaus et al. [5] for a 2D configuration. For the presented 3D simulations the axial and radial resolution are kept and only the circumferential resolution is varied. The final mesh consists of roughly 6.5 million cells. As can be seen in Fig. 3, the injection ele-

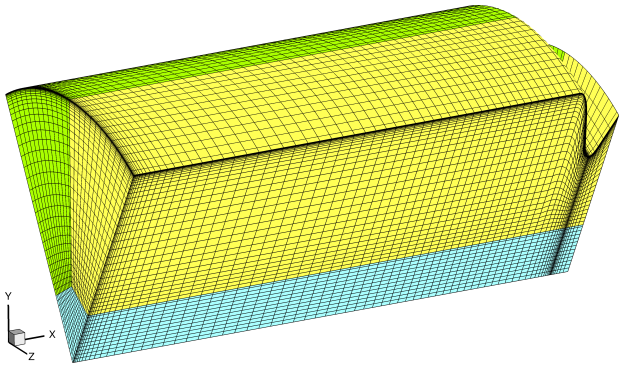

FIGURE 3. Utilized blocking strategy and mesh topology. Individual blocks represented by color. Geometry scaled and only every 4th grid line shown

ments are not resolved by the grid. Instead cells are identified as injection cell if their center of area is within the circle describing the element cross section. The resulting error in injection area is below 1%. An example for this mapping of injection cells is given in Fig. 4. An independent variation of the turbulent Prandtl Pr_t and Schmidt number Sc_t is performed and a setting of $Pr_t = 0.7$ and $Sc_t = 0.6$ is selected. On the injection pattern shown in Fig. 4, a mass flow boundary condition is enforced representing the total mass flow of 291 g/s measured in the experiments. Furthermore, an inlet turbulence intensity of $Tu = 0.07$ is prescribed as boundary condition without resolving the injector geometry. The combustion chamber walls are defined as non-slip hydraulic smooth walls. The faceplate is assumed to be adiabatic whereas on the combustion chamber wall a temperature profile from the experiment is prescribed. As the wall temperature has not been measured in the nozzle segment, the last experimentally obtained value is taken to prescribe a constant wall temperature further downstream of its position. A supersonic outlet boundary condition is chosen at the thrust chamber exit. All simulations use the SUPERBEE algorithm to obtain second order accuracy for the numerical flux computation. The employed settings for 2D Rocflam3 simulations differ only by the

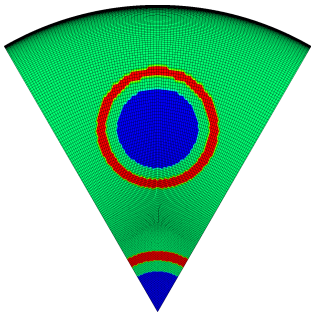

FIGURE 4. Mapping of inlet boundary condition to individual cells. Oxygen inflow in blue colored cells, methane inflow in red colored cells.

definition of a higher inlet turbulence intensity of $Tu = 0.2$. This is a consequence of the larger inflow area for an axisymmetric simulation when leaving the geometric injector dimensions unchanged. In order to compensate the lower inflow momentum in 2D, higher turbulence intensities are prescribed.

3.2. *Coolant Side*

The simulation of the coolant flow in the cooling channels and the heat conduction in the solid are performed with the commercial code Ansys CFX. The simulated domain is chosen such that it matches the hot gas wall of the combustion simulation, i.e. a 60° segment. A block structured mesh is chosen for both the fluid and the solid domain. The manifolds, i.e. inlet, outlet and transition manifolds, are only represented by their fluid volume. Furthermore, some simplifications of the geometry are made, e.g. drill tips where cooling channels and feed lines of circular cross section intersect are omitted. A section of the domain and an overview on the applied boundary conditions is given in Fig. 5.

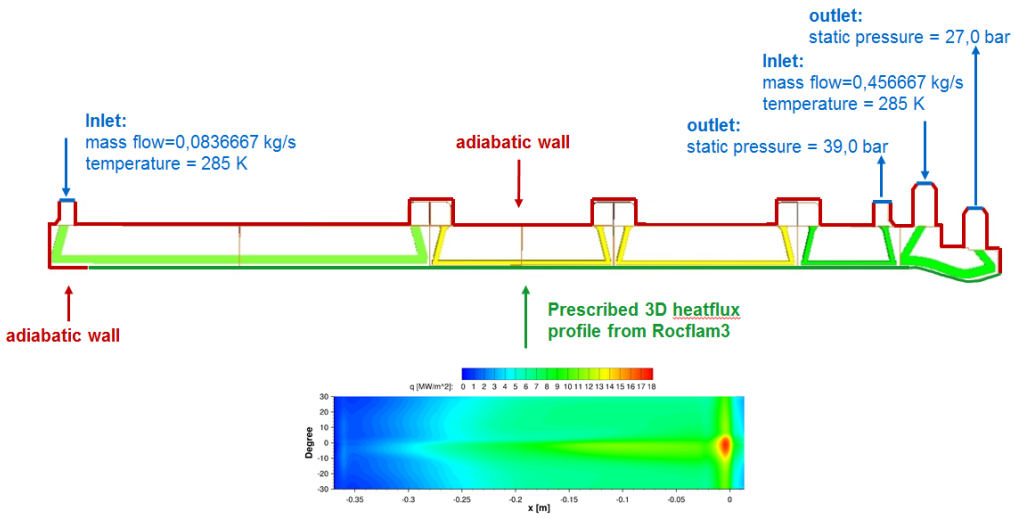

FIGURE 5. Boundary conditions of the coolant side

For each of the five combustion chamber segments separate meshes are created incorporating both the fluid and the solid domain of one representative cooling chan-

nel which yields a 10° segment for combustion chamber segments containing cooling channels with rectangular cross section and a 12° segment for combustion chamber segments containing cooling channels with circular cross section. In the final setup, five respectively six instances of each combustion chamber segment mesh are linked in circumferential direction and individual combustion chamber segments are linked axially using CFX's General Grid Interface (GGI).

For the coolant water a constant property fluid model is chosen, leading to an error in density of below 3% and an error in heat capacity below 0.3%. In the solid domain however, the heat conductivity of the OFHC-Cu is modeled as temperature dependent. Turbulence modeling is done using the SST model and the cooling channel walls are assumed to be hydraulic smooth surfaces. The heat transfer between individual combustion chamber segments is considered to be perfect, meaning any occurring contact resistance is neglected. Furthermore, radiation and natural convection on the outer surface of the combustion chamber is omitted

4. Results of the Hot Gas Side Simulations

The previously introduced Rocflam3 hot gas side simulation setting is applied to the defined test case of the Collaborative Research Center TRR40 Summer Program. Hereby, a wide range of results has been obtained employing 2D and 3D simulations. These are presented in the first of the following sections. Subsequently, the influence of the pressure tabulation within the flamelet framework and the turbulence modeling is discussed in more detail.

4.1. *Discussion of 2D and 3D Simulation Results*

Wall Heat Flux

A high fidelity in the wall heat flux prediction is a design critical factor and therefore of high importance at ArianeGroup. The results obtained for the test case of the summer program are shown in Fig. 6 in order to compare the 2D and 3D predictions to the experimentally obtained calorimetric data. For the comparison, the numerical results are averaged according to the water cooled segments of the thrust chamber resulting in the dashed curves. These show a good agreement to the test data for the first three segments covering a large portion of the cylindrical combustion chamber. However, larger deviations are observed for the remaining two segments. The numerical results do not show a local drop of the wall heat flux in the fourth segment together with a prediction of a lower peak heat flux values in the throat segment. This is currently not seen as a problem of the hot gas side simulation. It is assumed that the experimental conditions influence the obtained measurements as the structure and cooling channel simulations discussed later indicate.

Based on Fig. 6, certain differences occur between the 2D and 3D Rocflam3 simulations considering the solid lines representing the average values. Close to the faceplate following the injection of fuel and oxidizer, the 3D results predict a local heat flux peak which isn't observed in the 2D results. This can possibly be attributed to the presence of 3D flow phenomena, e.g. recirculation zones, close to the faceplate which are not correctly resolved in 2D when neglecting circumferential effects. A second major difference can be observed towards the end of the cylindrical combustion chamber as the 3D results give higher average heat flux values. This ongoing release of heat indi-

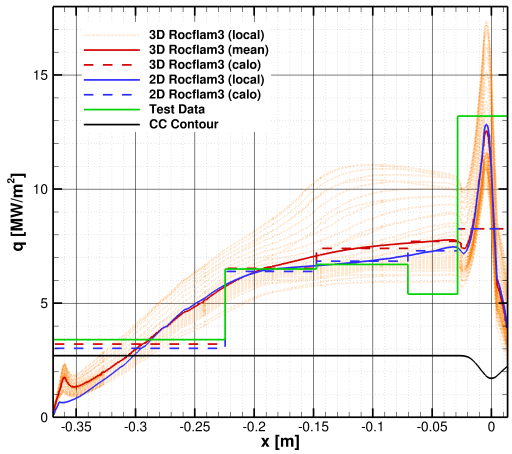

FIGURE 6. Wall heat flux obtained with 2D and 3D Rocflam3 simulations compared to the test data

cates an ongoing combustion process probably supported by the improved mixing when incorporating the 3-dimensional fluid dynamic effects. Looking further downstream, the predicted difference of the peak wall heat flux at $x = 0$ in the throat is negligible between the 2D and 3D simulation. The dotted lines in Fig. 6 show the circumferential distribution of the wall heat flux for the 3D simulation. It can be seen that compared to the average prediction, the local wall heat flux can be significantly higher. Therefore, 3D simulations are of high importance in a future rocket thrust chamber design process motivating the ongoing development of the Rocflam3 solver at ArianeGroup.

Circumferential Wall Heat Flux Distribution

In the following, a closer look is taken at the already introduced circumferential wall heat flux distribution. The distribution for the simulated 60° segment of the combustion chamber is shown in Fig. 7(a) confirming the importance of local peak heat flux predictions for estimating the design life of a rocket thrust chamber. For the current 3D Rocflam3 simulations, maximum wall heat flux values are observed at about 0° following the position of the injection element in the throat region. This is also shown by the extracted curves at certain distances from the faceplate as depicted in Fig. 7(b). The heat flux maximum remains at the injector position with a minimum towards a position between two injectors. However, the results shown in Fig. 7 reveal a significant deviation from the expected symmetry of the configuration. In order to solve this issue, efforts are currently underway to improve the flow modeling in Rocflam3 when applying the newly developed flamelet combustion model. The source of the assymetric flow field has been traced back to an issue in the flamelet library when using a logarithmic tabulation of the mixture fraction variance. Hereby, interpolation issues occur when approaching the upper variance limit.

Wall Pressure

In addition to the wall heat flux, experimental measurement data was obtained for the wall pressure along the combustion chamber axis. These are depicted together with the corresponding numerical predictions of the 2D and 3D Rocflam3 simulations in Fig. 8. Hereby, two normalization procedures are used to analyze different characteristics of

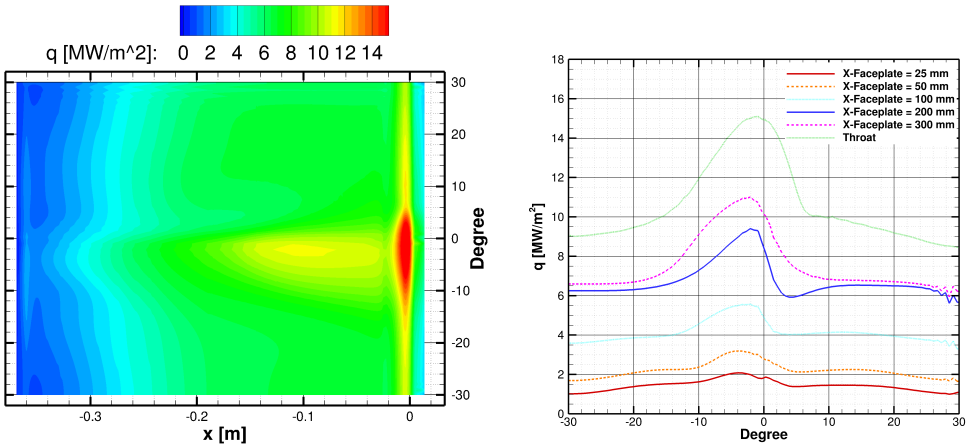

(a) Circumferential wall heat flux distribution

(b) Circumferential wall heat flux distribution at certain distances from the faceplate

FIGURE 7. Wall heat flux distribution on the combustion chamber wall for the 3D Rocflam3 simulation

the pressure profiles. In Fig. 8(a), all pressure values are normalized using the measurement value of 17.694 bar obtained at the position furthest downstream. The respective results show a under-prediction of the wall pressure in the range of 2-4 % for the numerical simulations with slightly higher pressure values obtained in the 2D simulation. In Fig. 8(b), each pressure profile is normalized with the corresponding pressure level at the measurement location furthest downstream. Thereby, the curvature of the pressure profiles can be compared to the experimental data revealing a better agreement for the 3D simulation results. The experimentally observed change in curvature is not predicted in the 2D simulation.

Average Combustion Chamber Temperature

The integral combustion chamber temperature for the numerical computations is shown in Fig. 9(a) correlating with the observations in regard to the wall heat flux profiles. The higher wall heat flux is a consequence of the higher chamber temperature, which in turn follows from the ongoing heat release due to chemical reactions. A second difference between the 2D and 3D simulation occurs for the first derivative of the temperature profiles. For the 2D simulation, the slope of the curve reduces gradually leading to a continous temperature increase along the cylindrical part of the combustion chamber. In contrast, a higher slope can be observed for the 3D simulation with a flattening of the profile towards the end. This pattern supports the higher maximum temperature in the 3D results. In summary, the integrated temperature profile indicates improved mixing for the 3D Rocflam3 simulation supporting the chemical reaction process, which leads to a higher combustion efficiency.

Average Combustion Chamber Composition

The indication of a higher combustion efficiency for the 3D computations given by the integral temperature profile is confirmed by the integral mass fraction profiles for the

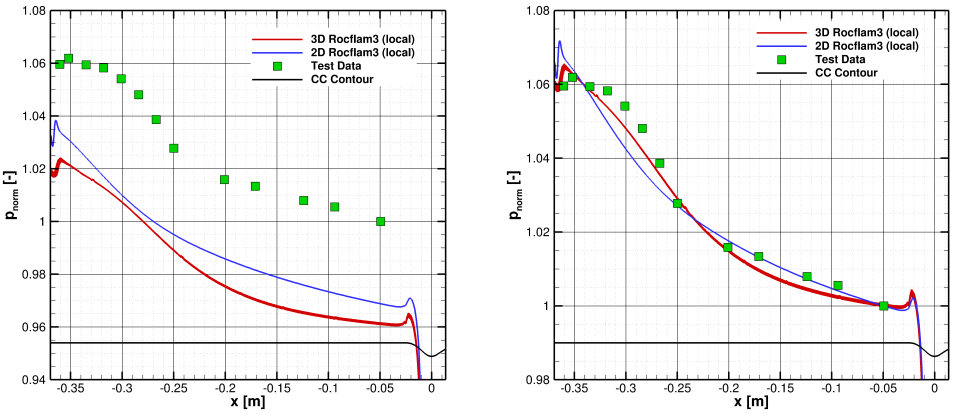

(a) Normalized for last experimental pressure level

(b) Normalized for individual pressure level at the last measurement position

FIGURE 8. Wall pressure obtained with 2D and 3D Rocflam3 simulations compared to the test data

fuel (dashed) and oxidizer (solid) shown in Fig. 9(b). Along the combustion chamber, more fuel and oxygen take part in the chemical reaction contributing to the increased local heat release compared to the 2D results. However, both simulations show that slightly more than 1 % of oxygen leaves the thrust chamber without taking part in the combustion process as the focus on the throat region in the upper-right part of Fig. 9(b) shows. This high degree of unburnt oxygen is most likely the main reason for the wall pressure under-estimation discussed previously as the full heat release contributing to a pressure build-up does not occur in the numerical computation. It is assumed that this can be attributed to the mixture based flamelet combustion model and deficiencies in modeling mixing processes in the current Rocflam3 setup. Further investigations are necessary on the 3D grid resolution and the turbulence modeling, which are decisive factors in the prediction of mixing phenomena.

Combustion Chamber Temperature Distribution

The flame structure and general flow field characteristics obtained for the summer program test case with the 3D Rocflam3 simulations are shown by the temperature distribution as given in Fig. 10. The temperature field is shown for a cut through the injector center plane at 0° and for a cut through the mid-plane between two injectors at 30°. For the upper cut in Fig. 10, the flame structure can be identified by the cold oxygen core and the stoiciometric mixture region indicated by the solid black line, for which high local temperatures are observed in a limited zone due to the chemical reaction. This zone of heat release is initiated at the post tip of the injection element as soon as the fuel and oxidizer streams start to mix. Comparing the two flames of the central and one outer injection element, it can be seen that the central flame is shorter. This might be a result of the flame - wall interaction as the enthalpy extraction towards the wall delays the chemical reaction progress. Furthermore, no immediate mixing of the two flame structures can be identified. The region between the two flames contains colder temperatures reaching about half-way into the combustion chamber. Only the high temperature region further

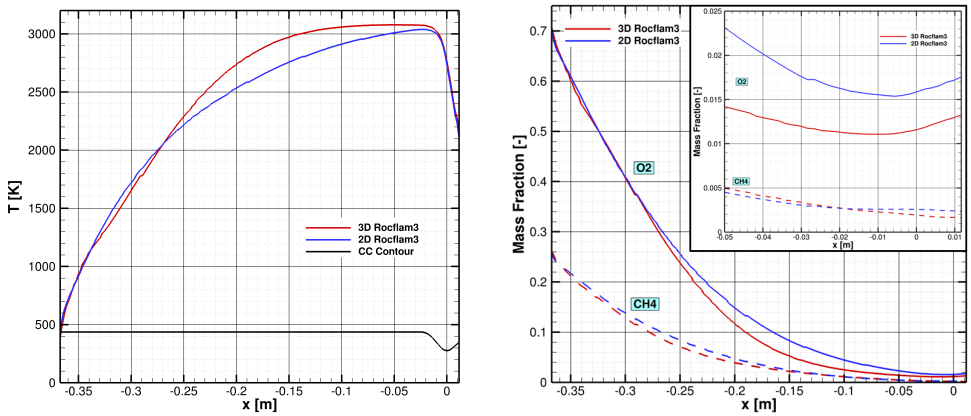

(a) Integrated temperature

(b) Integrated mass fractions of fuel and oxidizer (global and local in throat section)

FIGURE 9. Circumferentially and radially integrated profiles along the combustion chamber

downstream following the flames is fully mixed in regard to the fluid temperature. For the lower cut in Fig. 10, the influence of an injection element on the intermediate zone between two injectors is visible. The flame structure expands in circumferential direction leading to higher temperatures at the respective position at a 30° cut. In addition, a thicker thermal boundary layer is observed between two injector positions correlating with the previously discussed circumferential wall heat flux distribution.

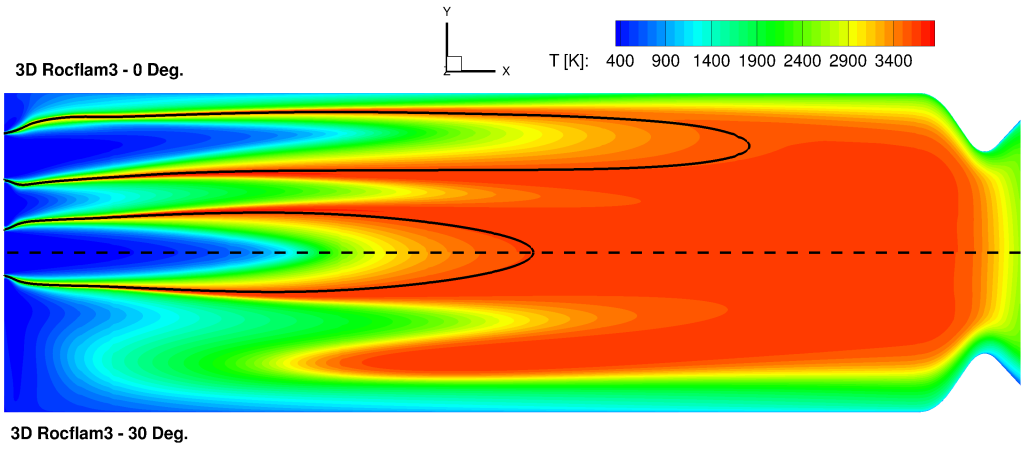

FIGURE 10. Temperature distribution for the 3D Rocflam3 simulation at 0° (injector center) and 30° (center between injectors)

4.2. *Influence of the pressure dependent chemistry tabulation*

In order to investigate the solution dependence of the pressure tabulation for the flamelet chemistry, two different setups are compared: the standard tabulation used for all simulations using 12 pressure levels covering the range from 0.1 bar to 20 bar; and a tab-

ulation using only 1 pressure level at 20 bar. The influence of the local fluid pressure on the composition is relevant in the throat an nozzle segment, over which the pressure drops from about 17 bar to 3 bar in the Rocflam3 simulations. A comparison between two 2D Rocflam3 simulations reveals that the pressure tabulation has a negligible influence on the wall heat flux profile. The wall pressure profile however is influenced by the pressure tabulation as shown in Fig. 11(a). While the curvature of the profile isn't influenced, the overall pressure level increases by 0.5 % approaching the experimental data. This is a consequence of a higher combustion efficiency and a higher heat release in the combustion chamber predicted with a single pressure tabulation. Another notable influence is observed for the fluid composition in the throat and nozzle section of the thrust chamber, especially when considering oxygen (blue) and water (red) as depicted in Fig. 11(b). As it can be seen, the switch to a single pressure tabulation has an inverting effect on the respective mass fractions. While the pressure resolved tabulation results in an increase of oxygen and a decrease of water across the nozzle, the slope of the profiles are maintained for a single pressure flamelet library. The observed behavior of the multi-pressure tabulation can be traced back to water decomposition, which is a thermally driven reaction process. As the pressure reduces from a composition perspective, the enthalpy is kept constant. Considering the phase diagram of water, a pressure drop at an approximately constant temperature leads to an increased overheating of the present water vapor. Ultimately, this initiates the decomposition reaction leading to the observed phenomenon in Fig. 11(b).

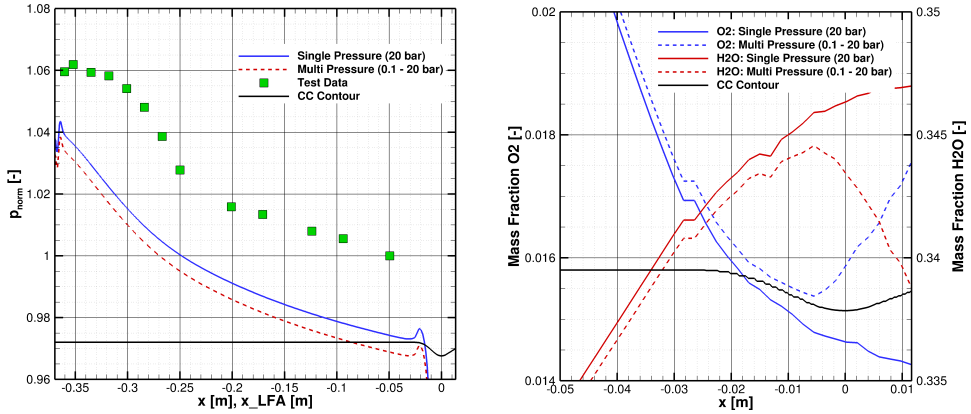

(a) Wall pressure profile

(b) Integrated mass fractions of O2 and H2O for the throat segment

FIGURE 11. Comparison of 2D Rocflam3 simulations using either a single (solid) or 12 (dashed) pressure level flamelet library

Concluding the remarks on the pressure tabulation, it has to be noted that multiple physical effects influence the composition in the throat and nozzle section. Apart from the pressure drop, the enthalpy significantly drops with the acceleration of the fluid to Mach numbers Ma $>$ 1. With the currently available chemistry tabulation methods, either zero or one out of two physical effects are accounted for in the simulations. It is therefore

the goal at ArianeGroup to further account for an enthalpy influence on the flamelet library to improve the numerical predictions.

4.3. *Evaluation of the turbulence modeling*

The discussion with other research teams during the Collaborative Research Center TRR40 Summer Program 2017 revealed that the mixing behavior can be improved by switching to an k-ϵ based turbulence model instead of Menter's k-ω-SST model. This is a promising approach to overcome the present deficiencies discussed in the first part of this section, which have been mainly attributed to an over-estimation of the unmixedness leading to a lower combustion efficiency by not using all the oxidizer injected into the combustion chamber. Therefore, the possibility of using the Launder - Sharma k-ϵ turbulence model [12] in Rocflam3 has been investigated for 2D simulations. The settings are only adapted for the turbulent Prandtl and Schmidt number by setting them as $Pr_t = 0.9$ and $Sc_t = 0.9$ while the remaining setup is unchanged. A comparison between the two turbulence models regarding the wall heat flux and the wall pressure is shown in Fig. 12. Considering the wall heat flux, certain improvements compared to the SST simulation can be observed. Using the k-ϵ model, the heat flux level remains constant over a larger portion of the combustion chamber following the main reaction zone after the faceplate. This agrees better with the experimental observations. Furthermore, a higher peak heat flux value in the throat region approaching the test data is predicted after switching the turbulence model. Considering the wall pressure profile, the curvature is now better predicted for the 2D simulation. However, an improvement in the prediction of the pressure level compared to the experimental data is not observed. This can be attributed to a small increase in the unmixedness when using k-ϵ formulation for the 2D simulation presenting no improvement. Summarizing the outcome, the usage of k-ϵ based turbulence model seems to be promising to further improve the predictive capabilities for the summer program test case at ArianeGroup. Therefore, a respective 3D simulation with further investigations is anticipated in the near future.

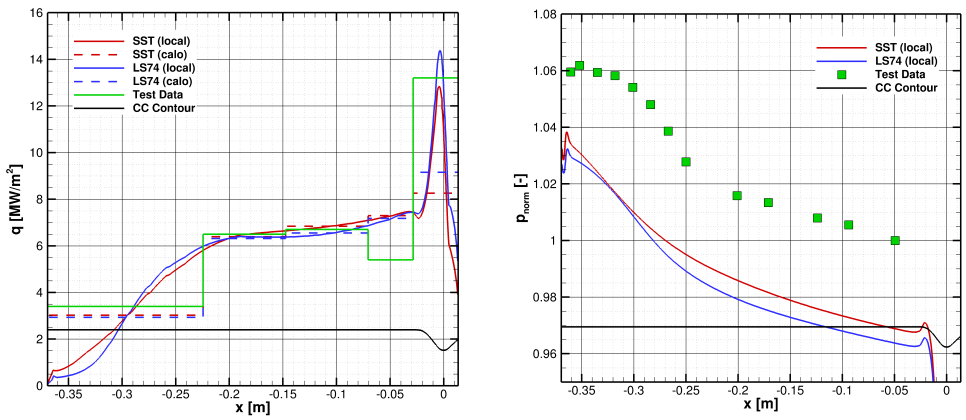

(a) Wall heat flux (b) Wall pressure

FIGURE 12. Comparison of Menter's k-ω-SST model and the Launder - Sharma k-ϵ turbulence model in Rocflam3 (2D)

The possibility of a higher stratification and an under-estimated mixing in the combustion chamber when employing Menter's k-ω-SST model for the considered test case might be attributed to the blending behavior of the turbulence model. The designed blending strategy intends to use a k-ω formulation in near wall regions to improve the boundary layer prediction while using a k-ϵ formulation in the core region of the flow. However, the geometric relations of the summer program test case are characterized by a large length to diameter ratio. This leads to the effect that the governing equations are solved employing a k-ω formulation for a large part of the combustion chamber, which might cause a higher unmixedness when using the SST model.

5. Results of the Structure & Coolant Side Simulations

The aforementioned setup of the structure and coolant side is used in a stand-alone simulation to get a first insight into the temperature distribution in the structure and the coolant heat up and pressure loss in the cooling channels. The obtained results are presented in the following section.

5.1. *Temperature Distribution in the Structure*

The temperature distribution in the combustion chamber structure is the main driver of life and thus has to be critically evaluated. The temperature field of both the structure and the coolant fluid is depicted in Fig. 13. A cut through all cooling channels is shown. The first four segments, cooled by the first cooling cycle, show a continuous increase of the hot gas wall temperature with the exception of regions in close proximity to the feeding lines of the cooling channels. There a decreased wall temperature can be observed. These regions coincide with a sharp local increase in coolant water temperature, e.g. at the downstream end of the first segment. This is assumed to be due to flow separation leading to local recirculation zones and increased flow velocities and thus heat transfer coefficient.

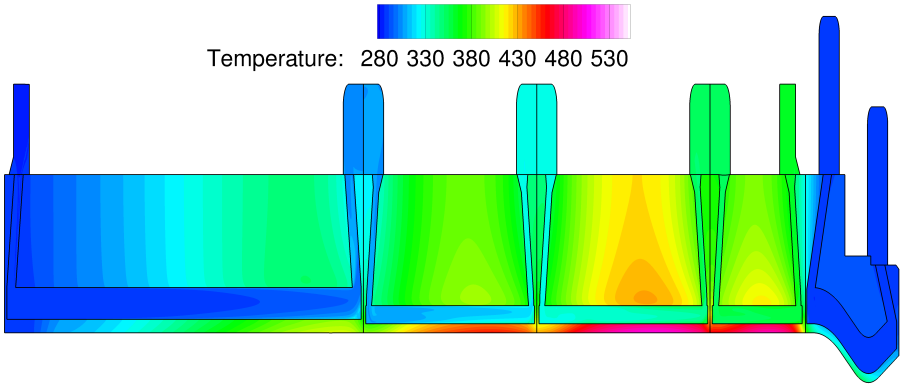

FIGURE 13. Section through the structure showing the temperature field

For the nozzle segment, cooled by the second cooling cycle, the radial temperature gradient is much more pronounced than the axial gradient. However, a strong temperature gradient can be observed at the interface of the last cylindrical segment and the nozzle segment. This can be explained with the difference in coolant mass flow and coolant temperature in the two segments. In the last cylindrical segment the cooling

water is already heated up significantly whereas in the nozzle segment cold coolant at 285 K enters the cooling channels. Furthermore, the coolant mass flow rate in the first cycle (0.502 kg/s) is much lower than in the second cycle (2.740 kg/s) and the total cross sectional area of the cooling channels in the nozzle segment (115.2 mm^2) is less than half the size of those in the cylindrical segments (378.0 mm^2). Hence, a higher flow velocity and thus a higher heat transfer coefficient is expected for the nozzle segment. This leads to a cold nozzle structure and thus a heat transfer from the last cylindrical segment to the nozzle segment.

A quantitative comparison of the measured experimental wall temperatures and the results achieved by numerical simulation is depicted in Fig. 14. The green squares represent the experimental data taken at hot gas wall distances between 0.7 and 1.5 mm. These values are used as boundary condition in the hot gas side simulations with Rocflam3. Due to the lack of experimental data in the nozzle segment the temperature from the last measured axial position is extrapolated, which is denoted by the open green square. The structure temperature from the simulation is evaluated at the same positions. The results are denoted by the orange crosses. A very good agreement between simulation and experiment is observed for the first segment. For the following segments, a high deviation occurs as the simulation overpredicts the temperature by more than 50 K.
This behavior is also reflected by the temperature on the hot gas wall directly above the injection element, indicated by the red line. It shows a generally increasing trend with local minima. These minima occur at the positions of cooling channel feed lines and are assumed to be due to local recirculation zones as explained above. It is expected that a better agreement of simulation and experiment can be achieved by future coupled simulations.

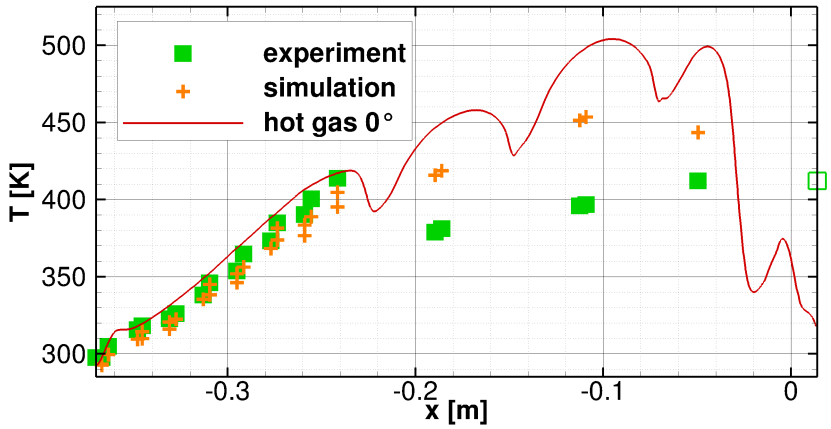

FIGURE 14. Wall temperature of the combustion chamber

Furthermore, it can be observed that the simulation predicts lower hot gas wall temperatures in the nozzle segment than the assumed boundary condition value of 412 K. Thus, the practice of using the temperature from the last measured axial position as wall boundary condition for the whole nozzle segment is questionable.

5.2. *Coolant Water*

The wall heat flux from the experiment is evaluated using the enthalpy change of the coolant water. Hence, the correct prediction of heat pick up and pressure loss are vital. A comparison of the volume averaged coolant water temperature in each manifold to the corresponding measured value from the experiment is shown in Fig. 15. It can be seen that the simulation agrees very well with the experimental data.

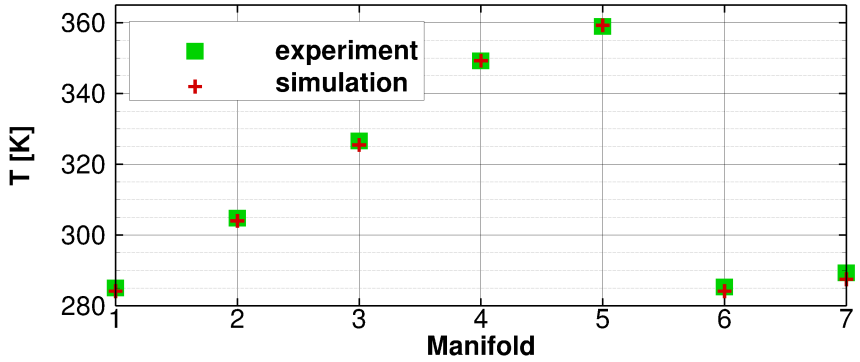

FIGURE 15. Temperature in the manifolds

The pressure drop over each cycle is given in table 2. As can be seen, the simulation overpredicts the pressure loss in both the cycles even though the simulation was performed using hydraulic smooth walls. It is assumed that the previously discussed flow separation has a significant impact on the pressure loss. The difference in pressure loss between experiment and simulation suggests that the actual hardware differs from the technical drawings and the sharp edges at the inlets and outlets were chamfered.

cycle	$\Delta p_{sim}[bar]$	$\Delta p_{exp}[bar]$
1 - cylinder	2,72	1,71
2 - nozzle	15,43	10,84

TABLE 2. Comparison of pressure loss for each cycle

However, an analysis of the enthalpy dependence on the pressure shows for the considered range of 40 bar +/- 10 bar a variance in enthalpy of lower than 2%.

With the volume averaged pressure and temperature in the manifolds the enthalpy is calculated using REFPROP [13]. The heat flux is obtained with the coolant mass flow rate $\dot{m}$ and the surface area A_{surf} using

$$\dot{q} = \dot{m} \cdot (h_{out} - h_{in})/A_{surf}. \tag{5.1}$$

A comparison of the heat flux evaluated from manifold data of the coolant side and structure simulation with Ansys CFX (red line), the heat flux evaluated from the standalone Rocflam3 simulation of the hot gas side (blue line) and the experimental reference

data (green line) is given in Fig. 16. As can be seen, a stand-alone hot gas side simulation cannot capture the heat flux profile in the fourth cylindrical and the nozzle segment. Only when resolving the combustion chamber structure and thus enabling axial heat conduction between the segments the decreasing heat flux in the fourth chamber segment is resolved. This in turn leads to an increased heat flux value in the nozzle segment. However, the nozzle heat flux is still underpredicted. As discussed above, the validity of the assumed wall temperature boundary condition is questionable and thus an improvement of the heat flux prediction is expected from a coupled simulation.

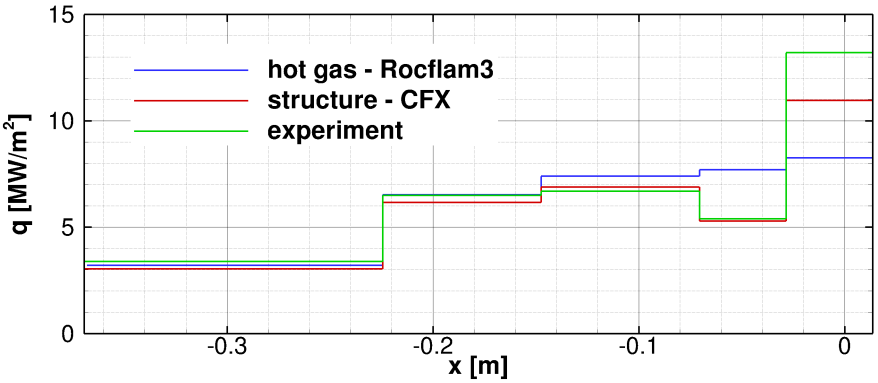

FIGURE 16. Heat flux evaluated in the coolant manifolds

6. Conclusions and Outlook

The ArianeGroup investigations within the Collaborative Research Center TRR40 Summer Program 2017 have revealed good results and mark a step forward towards better numerical predictions of CH4/O2 combustion in rocket thrust chambers. For both the wall heat flux and the wall pressure obtained experimentally, the numerical results are within acceptable limits. However, further research has to be done to improve the simulation framework in Rocflam3 to ensure high fidelity predictions of both characteristic values simultaneously. A first error has been identified in the summer program in regard to the handling of the mixture fraction variance in the newly developed flamelet model. This is currently being worked on during the validation process at ArianeGroup. Further studies on the turbulence modeling and the chemistry mechanism within the newly implemented flamelet framework are anticipated. Thereby, a wider range of test cases will be investigated in the future. In a next step, it is planned to extend the currently available flamelet approach by the incorporation of an enthalpy variable in the chemistry library. This is driven by the motivation to increase the fidelity of the wall heat flux predictions by accounting for a change in the species composition in the convectively cooled near wall region and across the expansion process through the throat and nozzle regions.

A major deficiency of the hot gas side simulations with Rocflam3 was observed in the wall heat flux prediction in the throat region. The heat flux drop upstream the nozzle and the high value are not predicted with the current simulation settings. In order to solve this issue, an improvement in the numerical simulations is expected with a coupling of the coolant and hot gas side in future simulations. As the initial structure and cooling channel simulations reveal, the nozzle segment is cooled significantly compared to the bordering

combustion chamber segment. Therefore, it is assumed that axial heat conduction in the coolant structure plays a major role in the experimental setup influencing the measured heat pickup in the distribution manifolds. Furthermore, the currently used approach of setting the last experimentally measured wall temperature value as constant for the nozzle segment is likely a wrong assumption. Thus, an evaluation of the heat flux from a stand-alone hot gas side simulation cannot match the experimental results.

Acknowledgments

The analysis of the 7-element sub-scale combustion chamber performed in the summer program of the Sonderforschungsbereich Transregio 40 is financed by ArianeGroup (sponsored by the German Space Agency, DLR Bonn, within the National technology program TARES 2020 under contract No. 50RL1710). In addition, the investigations are supported in the frame of a project sponsored by the Bayerische Forschungsstiftung within the project "Umweltfreundliche Treibstoffkombination LOX/Methan".

References

[1] PRECLIK, D., HAGEMANN, G., KNAB, O., BRUMMER, L., MÄDING, C., WIEDMANN, D. AND VUILLERMOZ, P. (2005). LOX/Hydrocarbon Propellant Trade Considerations for Future Reusable Liquid Booster Engines. In: *41st AIAA/ASME/SAE/ASEE Joint Propulsion Conference & Exhibit*. Tucson, Arizona.

[2] STRUNZ, R., HAGEMANN, G., GRAUER, F., BRUMMER, L., PRECLIK, D., BIOJOUX, E., VIOT, X., DANTU, G., STAFFILANO, U., CUOCO, F. AND SANTILLI, M. (2006). Main Stage Liquid Propulsion Activities within Europe's future Launcher Prepatory Programme FLPP. In: *42nd AIAA/ASME/SAE/ASEE Joint Propulsion Conference & Exhibit*. Sacramento, California.

[3] BLASI, R. AND HÄBERLE, J. (2016). LOX/Methane Thrust Chamber Demonstrator Testing. In: *Space Propulsion Conference*. Rome, Italy.

[4] TCHOU-KIEN, D., IANETTI, A., GIRARD, N., BONHOMME, C., RAVIER, N. AND EDELINE, E. (2017). PROMETHEUS, a low cost LOX/CH4 Engine Prototype. In: *53rd AIAA/SAE/ASEE Joint Propulsion Conference*. Atlanta, Georgia.

[5] EIRINGHAUS, D., RAHN, D., RIEDMANN, H., KNAB, O. AND HAIDN, O. (2017). Numerical Investigation of a 7-Element GOX/GCH4 Subscale Combustion Chamber. In: *7th European Conference for Aeronautics and Aerospace Sciences (EUCASS)*. Milano, Italy.

[6] MAGNUSSEN, B.F. (2005). The Eddy Dissipation Concept A Bridge betweeen Science and Technology. In: *ECOMAS Thematic Conference on Computational Combustion*. Lissabon, Portugal.

[7] RIEDMANN, H., GÖRGEN, J., IVANCIC, B., MAKOWKA, K. AND FREY, M. (2016). Numerical SImulation of the Hot Gas Side Flow and Wall Heat Transfer in CH4/O2 Rocket Thrust Chambers. In: *Space Propulsion 2016*.

[8] ROTH, C., HAIDN, O., CHEMNITZ, A., SATTELMAYER, T., DAIMON, Y., FRANK, G., MÜLLER, H., ZIPS, J., PFITZNER, M., KELLER, R., GERLINGER, P., MAESTRO, D., CUENOT, B., RIEDMANN, H. AND SELLE, L. (2016). Numerical Investigation of Flow and Combustion in a Single-Element GCH4/GOX Rocket Combustor. In: *52nd AIAA/SAE/ASEE Joint Propulsion Conference*.

[9] SILVESTRI, S., CELANO, M., SCHLIEBEN, G. AND HAIDN, O. (2016). Characterization of a Multi-Injector GOX-GCH4 Combustion Chamber. In: *52nd AIAA/SAE/ASEE Joint Propulsion Conference*. Salt Lake City, Utah.

[10] MENTER, F.R. (1994). Two-Equation Eddy-Viscosity Turbulence Models for Engineering Applications. *AIAA Journal*, **32**(8), 1598–1605.

[11] PETERS, N. (1986). Laminar flamelet concepts in turbulent combustion. In: *21st Symposium on Combustion*. 1231–1250.

[12] LAUNDER, B.E. AND SHARMA, B.I. (1974). Applications of the Energy-Dissipation Model Turbulence to the Calculation of Flow near a Spinning Disc. *Letters in Heat and Mass Transfer*, **1**, 131–138.

[13] LEMMON, E., HUBER, M. AND MCLINDEN, M. (2008). *NIST Standard Reference Database 23: Reference Fluid Thermodynamic and Transport Properties - REFPROP, Version 8.0*. National Institute of Standards and Technology, Gaithersburg.